Turkish Journal of Engineering & Environmental Sciences

http://journals.tubitak.gov.tr/engineering/

Research Article

Turkish J Eng Env Sci
(2014) 38: 51 – 63

doi:10.3906/muh-1309-17

Effects of radiation–conduction interaction on mixed convection from a vertical cone embedded in a porous media with high porosity

Ahmet KAYA*
Department of Mechanical Engineering, Faculty of Engineering, Kahramanmaraş Sütçü İmam University, Kahramanmaraş, Turkey

Received: 18.09.2013 • **Accepted:** 07.07.2014 • **Published Online:** 24.10.2014 • **Printed:** 21.11.2014

Abstract: The problem of steady laminar mixed convection heat transfer about a vertical cone embedded in a porous medium with high porosity was studied numerically, taking into account the radiation–conduction effect. The fluid was assumed to be incompressible and dense. The nonlinear coupled parabolic partial differential equations governing the flow were transformed into nonsimilar boundary layer equations, which were then solved numerically using the Keller box method. The effects of the exponent in the power law variation of the free stream velocity m, the mixed convection parameter Ri, the radiation–conduction parameter R_d, the surface temperature parameter θ_w, and Forchheimer parameter γ on the velocity and temperature profiles, as well as on the local skin friction and local heat transfer, are presented and analyzed. The validity of the methodology and analysis was checked by comparing the results obtained for some specific cases with those available in the literature.

Key words: Thermal radiation, mixed convection, cone, porous media

1. Introduction

Thermal buoyancy-induced flow and convective heat transfer in fluid-saturated porous media is encountered in many engineering problems, such as the design of pebble-bed nuclear reactors, catalytic reactors and compact heat exchangers, geothermal energy conversion, fibrous material use in the thermal insulation of buildings, heat transfer from storage of agricultural products that generate heat as a result of metabolism, petroleum reservoirs, or storage of nuclear wastes [1]. Comprehensive reviews of papers on this topic have been presented by Cheng [2,3], Pop et al. [4], Nield and Bejan [5], Vafai [6], Pop and Ingham [7], and Ingham and Pop [8].

Convective heat transfer over a stationary cone is important for the thermal design of various types of industrial equipment, such as heat exchangers, canisters for nuclear waste disposal, nuclear reactor cooling systems, or geothermal reservoirs [9]. In recent years, several investigators have studied natural and mixed convection flows over a cone with and without porous media. Ravindran et al. [9] obtained a nonsimilar solution of a steady mixed convection flow over a vertical cone with surface mass transfer (injection or suction) when the axis of the cone was in line with the flow. Roy et al. [10] obtained a nonsimilar solution of an unsteady mixed convection flow over a vertical cone in the presence of surface mass transfer. Osalusi et al. [11] studied the effect of combined viscous dissipation and Joule heating on unsteady mixed convention magnetohydrodynamic flow on a rotating cone in an electrically conducting rotating fluid in the presence of Hall and ionslip currents. Ece [12] investigated the laminar free-convection boundary layer flow in the presence of a transverse magnetic field

*Correspondence: ekaya38@gmail.com

over a vertical down-pointing cone with mixed thermal boundary conditions. Roy and Anilkumar [13] obtained a semisimilar solution of an unsteady mixed convection flow over a rotating cone in a rotating viscous fluid when the free stream angular velocity and the angular velocity of the cone varied arbitrarily with time. For porous media, Kumari and Nath [1] studied the non-Darcy natural convention flow of Newtonian fluids on a vertical cone embedded in a saturated porous medium with power-law variation of the wall temperature/concentration or heat/mass flux and suction/injection with the streamwise distance x. Yih [14] investigated the radiation effect on the mixed convection flow of an optically dense viscous fluid adjacent to an isothermal cone embedded in a saturated porous medium with Rosseland diffusion approximation. Grosan et al. [15] studied steady free convection boundary layers over a vertical cone embedded in a porous medium filled with a non-Newtonian fluid with an exponential decaying internal heat generation. Cheng [16] studied the Soret and Dufour effects on boundary layer flow due to natural convection heat and mass transfer over a downward-pointing vertical cone in a porous medium saturated with Newtonian fluids with constant wall temperature and concentration.

In most of the studies in the literature, the problem of the cone has been taken as natural convection. However, it is discussed as a mixed convection problem in this study. Furthermore, the effect of radiation–conduction on mixed convection flow over a vertical cone embedded in a porous medium with uniform surface temperature has been analyzed. The free stream velocity is assumed to have power-law variation with the distance measured from the vortex of the cone. Nonsimilar solutions are obtained numerically by solving a set of coupled nonlinear partial differential equations using an implicit finite difference scheme (Keller box method).

2. Analysis

Consider steady, incompressible, laminar, Newtonian, 2-dimensional, radiative heat transfer from an isothermal cone with a half angle α embedded in a porous medium. Far above and below the surfaces of the cone, the velocity and the temperature of the free stream are U_e and T_∞, respectively. The streamwise coordinate x is measured from the apex of the cone along its generator, and the transverse coordinate y is measured normal to it into the fluid, respectively (Figure 1). The corresponding velocity components in the x and y directions are u and v, respectively. The surface of the cone is held at a uniform temperature T_w, which is higher than the ambient fluid temperature T_∞. The porous medium is assumed to be transparent and in thermal equilibrium with the fluid. Both the fluid and the porous medium are opaque for self-emitted thermal radiation. The properties of the fluid and the porous media, such as viscosity, thermal conductivity, specific heat, and permeability, are assumed to be constant. The porous medium is considered to be homogeneous and isotropic (i.e. uniform with a constant porosity and permeability). Furthermore, the fluid is assumed to be gray, emitting and absorbing heat but not scattering it. We assume the radiative heat flux in the x direction is considered negligible in comparison with that in the y direction.

The governing equations for this investigation are based on the usual boundary layer equations modified to include the porous medium effects and the thermal buoyancy effects. These equations (with the Boussinesq and non-Darcy approximations) can be written as follows [17,18].

$$\frac{\partial (ur)}{\partial x} + \frac{\partial (vr)}{\partial y} = 0 \tag{1}$$

$$\frac{1}{\varepsilon^2}\left[u\frac{\partial u}{\partial x} + v\frac{\partial u}{\partial y}\right] = U_e\frac{\partial U_e}{\partial x} + \frac{\nu}{\varepsilon}\frac{\partial^2 u}{\partial y^2} + g\beta\left(T - T_\infty\right)\cos\alpha - \frac{\nu}{K}\left(u - U_e\right) - \frac{F}{K^{1/2}}\left(u^2 - U_e^2\right) \tag{2}$$

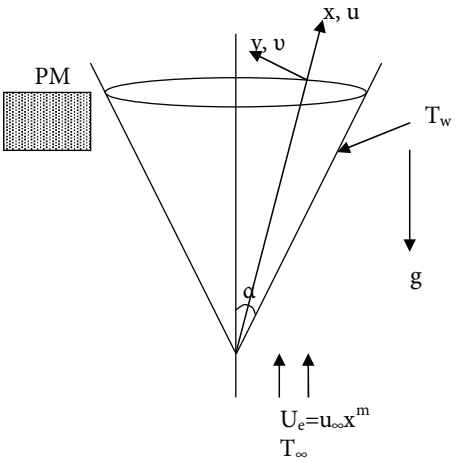

Figure 1. The schematic of the problem.

$$u\frac{\partial T}{\partial x}+\upsilon\frac{\partial T}{\partial y}=\frac{k_e}{\rho c_p}\frac{\partial^2 T}{\partial y^2}-\frac{1}{\rho c_p}\frac{\partial}{\partial y}\left(q_R\right) \tag{3}$$

The above equations are called the Brinkman–Forchheimer–extended Darcy equations [19]. Here, u and υ are the velocity components in the x and y directions, respectively; $U_e = u_\infty x^m$ is the free stream velocity; m is the free stream velocity component; T is the temperature of the fluid; υ is the kinematic viscosity; ρ is the fluid density; g is the acceleration due to gravity; α is the half angle of the cone; r is the radius of the cone; ε is the porosity; K is the permeability; F is the inertial coefficient, which depends on the permeability and microstructure of the porous matrix; and k_e is the effective thermal conductivity of the porous medium. The thermal dispersion effect is minimal when the thermal diffusivity ($k_e/\rho c_p$) of the porous matrix is of the same order of magnitude as that of the working fluid. Assuming that the effective thermal diffusivity remains constant when the porosity of the porous medium varies with the normal distance is a viewpoint shared by many other investigators [18].

The quantity q_R on the right-hand side of Eq. (3) represents the radiative heat flux in the y direction. For simplicity and comparison, the radiative heat flux term in the energy equation is analyzed by utilizing the Rosseland diffusion approximation [20] for an optically thick boundary layer as follows:

$$q_r=-\frac{4\sigma}{3\alpha_R}\frac{\partial T^4}{\partial y} \text{ and } \frac{\partial q_r}{\partial y}=-\frac{16\sigma}{3\alpha_R}\frac{\partial}{\partial y}\left(T^3\frac{\partial T}{\partial y}\right), \tag{4}$$

where σ is the Stefan–Boltzmann constant and α_R is the Rosseland mean absorption coefficient. This approximation is valid at points optically far from the bounding surface and is good only for intensive absorption, i.e. for an optically thick boundary layer [21].

The appropriate boundary conditions for the velocity and temperature of this problem are:

$$\left.\begin{array}{llll} x=0, & y>0, & T=T_\infty, & u=U_e=u_\infty x^m \\ x>0, & y=0, & T=T_w, & u=0, \upsilon=0 \\ y\to\infty, & & T\to T_\infty & u\to U_e=u_\infty x^m \end{array}\right\}, \tag{5}$$

where m is the exponent in the power law variation of the free stream velocity.

Because the boundary layer thickness is small, the local radius to a point in the boundary layer r can be represented by the local radius of the vertical cone [22]:

$$r = xSin\left(\alpha\right). \tag{6}$$

To seek a solution, the following dimensionless variables are introduced:

$$\xi = \frac{vx}{KU_e}, \psi\left(x,y\right) = \left(vU_e x\right)^{1/2} f(\xi,\eta), \quad \eta = y\left(\frac{U_e}{vx}\right)^{1/2}, \theta = \frac{T-T_\infty}{T_w - T_\infty}, \gamma = \frac{FK^{1/2}U_e}{v}, \tag{7}$$

where $\psi(x,y)$is the free stream function that satisfies Eq. (1) with $ru = \partial\psi/\partial y$ and $rv = -\partial\psi/\partial x$.

In terms of these new variables, the velocity components can be expressed as

$$u = U_e f', \tag{8}$$

$$v = -\left(\frac{U_e v}{x}\right)^{1/2}\left\{\frac{m+1}{2}f + \left(1-m\right)\xi\frac{\partial f}{\partial\xi} + \frac{\left(m-1\right)\eta}{2}f'\right\}. \tag{9}$$

The transformed momentum and energy equations, together with the boundary conditions Eqs. (2), (3), and (5), can be written as

$$\begin{array}{l} \frac{1}{\varepsilon}f''' + \frac{1}{\varepsilon^2}\left(\frac{m+1}{2}\right)ff'' + \frac{m}{\varepsilon^2}\left(1-f'^2\right) + Ri\theta\xi - \xi\left(f'-1\right) - \gamma\xi\left(f'^2-1\right) = \\ \frac{(1-m)\xi}{\varepsilon^2}\left(f'\frac{\partial f'}{\partial\xi} - f''\frac{\partial f}{\partial\xi}\right) \end{array}, \tag{10}$$

$$\frac{1}{\Pr}\theta'' + \frac{m+1}{2}f\theta' + \frac{4}{3\Pr R_d}\left[\left(\theta\left[\theta_w - 1\right]+1\right)^3\theta'\right]' = \left(1-m\right)\xi\left(f'\frac{\partial\theta}{\partial\xi} - \theta'\frac{\partial f}{\partial\xi}\right), \tag{11}$$

with the following boundary conditions:

$$\left.\begin{array}{lll} f\left(\xi,0\right) + \left[\frac{2(1-m)}{1+m}\right]\xi\frac{\partial f}{\partial\xi} = 0, & f'\left(\xi,0\right) = 0, & \theta\left(\xi,0\right) = 1 \\ & f'\left(\xi,\infty\right) = 1, & \theta\left(\xi,\infty\right) = 0 \end{array}\right\}. \tag{12}$$

The corresponding dimensionless groups that appear in the governing equations are defined as:

$$\Pr = \frac{\mu c_p}{k} = \frac{v}{\alpha}, \quad \gamma = \frac{FK^{1/2}U_e}{v}, \quad Ri = \frac{Gr_K}{Re_K}, \quad Gr_K = \frac{g\beta\left(T_w - T_\infty\right)K^{3/2}\cos\alpha}{v^2}, \quad Re_K = \frac{U_e K^{1/2}}{v},$$

$$R_d = \frac{k\alpha_R}{4\sigma T_\infty^3}, \quad \theta_w = \frac{T_w}{T_\infty}, \tag{13}$$

where Pr is the Prandtl number, γ is the Forchheimer parameter, and Ri is the Richardson number, which measures the relative importance of free to forced convection. Ri = 0 corresponds to the case of purely forced convection conditions. Ri $\to\infty$ corresponds to the case of purely free convection conditions. It is noted that Ri is not the function of x. Gr_K is the average modified Grashof number based on permeability K, Re_K is the averaged Reynolds number based on permeability K, R_d is the Planck number (radiation–conduction parameter), and θ_w is the surface temperature ratio to the ambient fluid.

In the above system of equations, the radiation conduction parameter is absent from the mixed convection heat transfer problem when $\mathrm{R}_d \to \infty$. It should be mentioned that the optically thick approximation should

be valid for relatively low values of the radiation–conduction parameter, R_d. According to Ali et al. [23], some values of R_d for different gases are: (1) R_d= 10–30: carbon dioxide (37.78–343.33 °C) with the corresponding Prandtl number range of 0.76–0.6; (2) R_d= 30–200: ammonia vapor (48.89–204.44 °C) with the corresponding Prandtl number range of 0.88–0.84; (3) R_d= 30–200: water vapor (104.44–482.22 °C) with the corresponding Prandtl number of 1.

3. Numerical solution

The system of transformed equations under the boundary conditions of Eqs. (10) and (11) has been solved numerically using the Keller box scheme along with Newton's linearization technique, which has proven to be an efficient and accurate finite-difference scheme [24]. In this method, any quantity g at point (ξ_n, η_j) is written as g_j^n. Quantities and derivatives at the midpoints of grid segments are approximated to the second order as

$$g_j^{n-1/2} = \frac{1}{2}\left(g_j^n + g_j^{n-1}\right), \quad g_{j-1/2}^n = \frac{1}{2}\left(g_j^n + g_{j-1}^n\right) \tag{14}$$

$$\left(\frac{\partial g}{\partial \xi}\right)_j^{n-1/2} = \frac{1}{\Delta\xi}\left(g_j^n - g_j^{n-1}\right), \quad (g')_{j-1/2}^n = \frac{1}{\Delta\eta}\left(g_j^n - g_{j-1}^n\right), \tag{15}$$

where g is any dependent variable and n and j are the node locations along the ξ and η directions, respectively. First, the third-order partial differential equation is converted in the first order by substitutions $f' = s$ and $s' = w$. The difference equations that are to approximate the previous equations are obtained by averaging about the midpoint $\left(\xi_n, \eta_{j-1/2}\right)$, and those that are to approximate the resulting equations are obtained by averaging about $\left(\xi_{n-1/2}, \eta_{j-1/2}\right)$. At each line of constant ξ, a system of algebraic equations is obtained. With the nonlinear terms evaluated at the previous station, the algebraic equations are solved iteratively [25]. The same process is repeated for the next value of ξ and the problem is solved line by line until the desired ξ (ξ is taken as 2 for this study) value is reached. The effect of the grid size $\Delta\eta$ and $\Delta\xi$ and the edge of the boundary layer η_∞ (η_∞ is taken as 16 for this study) on the solution was examined. The results presented here are independent of the grid size.

In the calculations, a uniform grid of the step size 0.01 in the η-direction and a nonuniform grid in the ξ-direction with a starting step size of 0.1 and an increase of 0.1 times the previous step size were found to be satisfactory in obtaining sufficient accuracy. For a given value of ξ, the iterative procedure is stopped when the difference in computing the velocity and the temperature in the next iteration is less than 10^{-6}, i.e. when $|\delta f_i| \leq 10^{-6}$, where the superscript denotes the iteration number. The details of the computational procedure were discussed further by Cebeci and Bradshaw [24] and Takhar and Beg [26].

In order to verify the accuracy of the present method, the present results were compared with those of Lloyd and Sparrow [27] and Chang [28]. The comparison was found to be in good agreement, as shown in the Table.

4. Results and discussion

In this paper, a 2-dimensional steady mixed convection flow over an isothermal cone in the presence of thermal radiation has been analyzed in porous medium with high porosity. The free stream velocity varies according to the power function of distance m. The following ranges of the main parameters are considered: Pr = 1.0; porosity ε = 0.98; free stream velocity exponent m = 0.0, 0.1, 0.2, 0.3, and 0.4; mixed convection parameter

Table. Comparison of the values-$\theta'(\xi,0)$ for various values of ξ, with $\varepsilon = 1$, Pr = 10, $\gamma = 0$, m = 0, $\alpha = 0$, $R_d \to \infty$, and $\theta_w = 0.0$.

ξ	Lloyd and Sparrow [27]	Chang [28]	Present study
0.00000	0.7281	0.7280	0.7278
0.00125	0.7313	0.7291	0.7291
0.00500	0.7404	0.7373	0.7328
0.01250	0.7574	0.7566	0.7556
0.05000	0.8259	0.8351	0.8351
0.12500	0.9212	0.9412	0.9432
0.25000	1.0290	1.0603	1.0603

Ri = 0, 1, 5, and 10; Forchheimer parameter $\gamma = 1.5$, 2.5, and 3.5; radiation–conduction parameter R_d= 30, 50, and 100; and surface temperature ratio $\theta_w = 1.7$, 2.0, and 2.3. The effects of free stream velocity exponent m, the mixed convection parameter Ri, the radiation parameter R_d, the surface temperature ratio θ_w, and the Forchheimer parameter γ on momentum and heat transfer are analyzed and discussed.

Figure 2 shows the dimensionless velocity and temperature profiles inside the boundary layers for different values of the free stream velocity exponent m. Increasing the free stream velocity exponent m increases momentum (Figure 2a) and decreases thermal boundary layer thickness (Figure 2b).

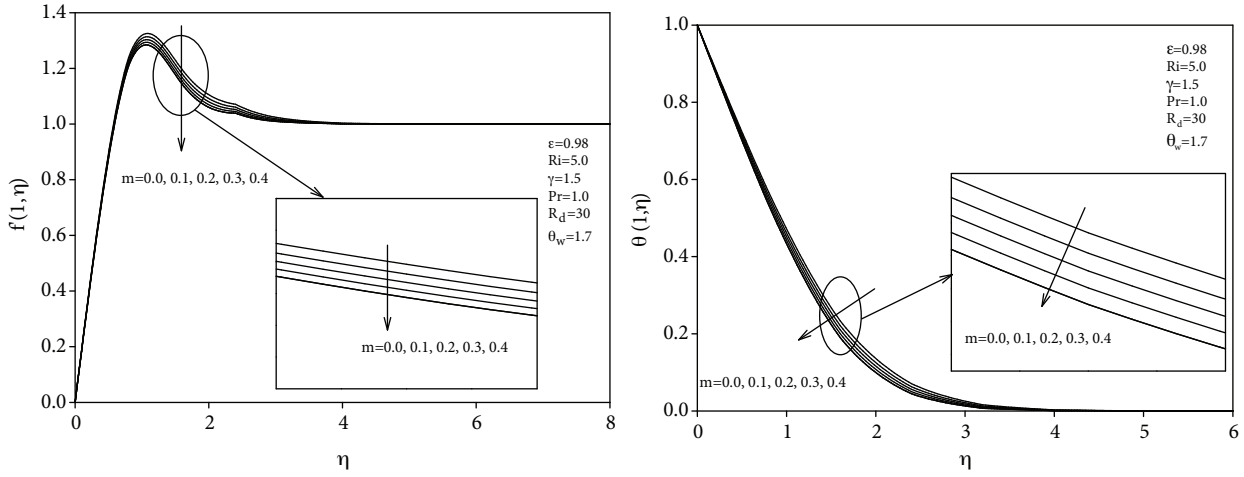

Figure 2. a) Dimensionless velocity profiles for different values of m while Pr = 1.0, $\varepsilon = 0.98$, Ri = 5, $\gamma = 1.5$, R_d = 30, $\theta_w = 1.7$, and $\xi = 1.0$. b) Dimensionless temperature profiles for different values of m while Pr = 1.0, $\varepsilon = 0.98$, Ri = 5, $\gamma = 1.5$, $R_d = 30$, $\theta_w = 1.7$, and $\xi = 1.0$.

Furthermore, increasing the free stream velocity exponent m increases local skin friction (Figure 3a) and local heat transfer parameters (Figure 3b).

Figure 4 shows the effect of Ri on the dimensionless velocity and temperature profiles for m = 0 and 0.2. As Ri increases, free convection is enhanced near the boundary, which gives rise to greater velocities inside the boundary layer (Figure 4a). With regard to temperature profile, the temperature gradient at the wall increases as Ri increases, with an accompanying decrease in thermal boundary layer thickness (Figure 4b) indicating a larger heat transfer rate. Increasing the free stream velocity exponent m also decreases velocity profile and increases temperature profile at the wall (i.e. y = 0).

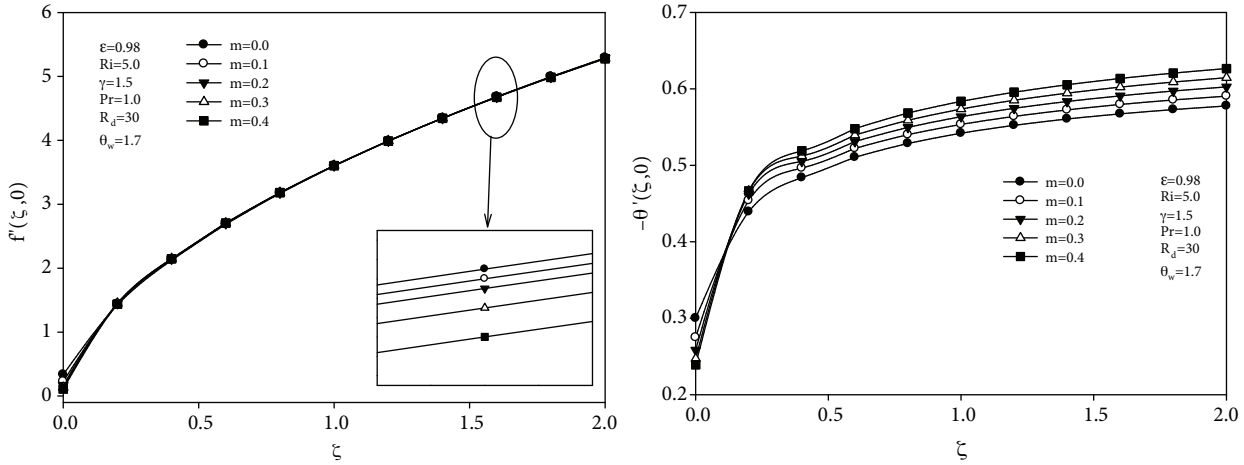

Figure 3. a) Numerical values of local skin friction parameter against the streamwise distance ξ for different values of m while Pr = 1.0, ε = 0.98, Ri = 5, γ = 1.5, R_d = 30, and θ_w = 1.7. b) Numerical values of local heat transfer parameter against the streamwise distance ξ for different values of m while Pr = 1.0, ε = 0.98, Ri = 5, γ = 1.5, R_d = 30, and θ_w = 1.7.

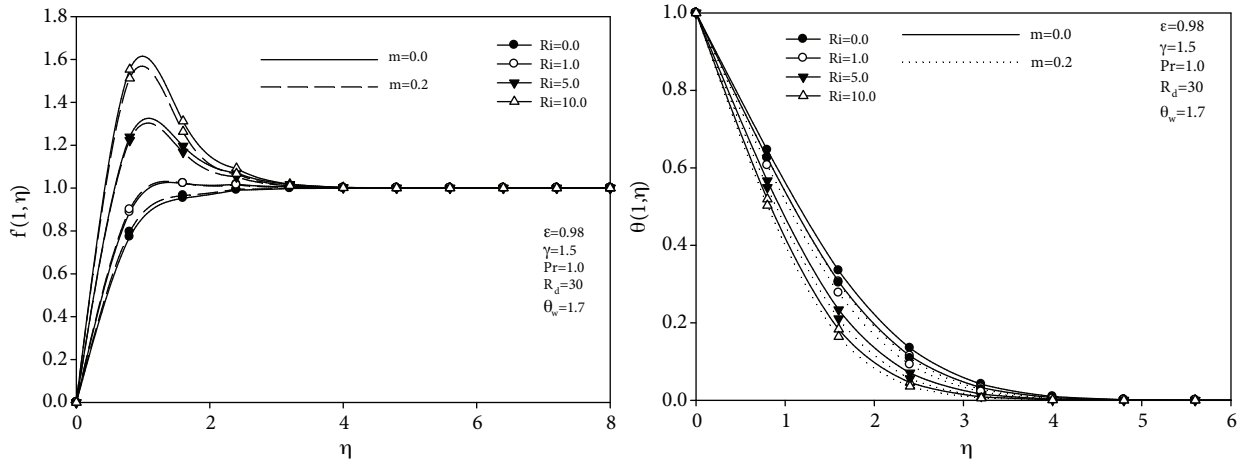

Figure 4. a) Dimensionless velocity profile for different values of Ri and m while Pr = 1.0, ε = 0.98, γ = 1.5, R_d = 30, θ_w = 1.7, and ξ = 1.0. b) Dimensionless temperature profile for different values of Ri and m while Pr = 1.0, ε = 0.98, γ = 1.5, R_d = 30, θ_w = 1.7, and ξ = 1.0.

The effects of mixed convection parameter Ri on the local skin friction and the local heat transfer parameters are shown in Figure 5. Both the local skin friction (Figure 5a) and the local heat transfer (Figure 5b) increase with an increase in mixed convection parameter Ri.

Figure 6 shows the dimensionless velocity and temperature profiles inside the boundary layer for different values of the radiation parameter R_d and free stream velocity exponent m. Increasing R_d and free stream velocity exponent m increases the momentum boundary layer thickness (Figure 6a) and decreases the temperature boundary layer thickness (Figure 6b) (i.e. increases temperature gradients at the wall).

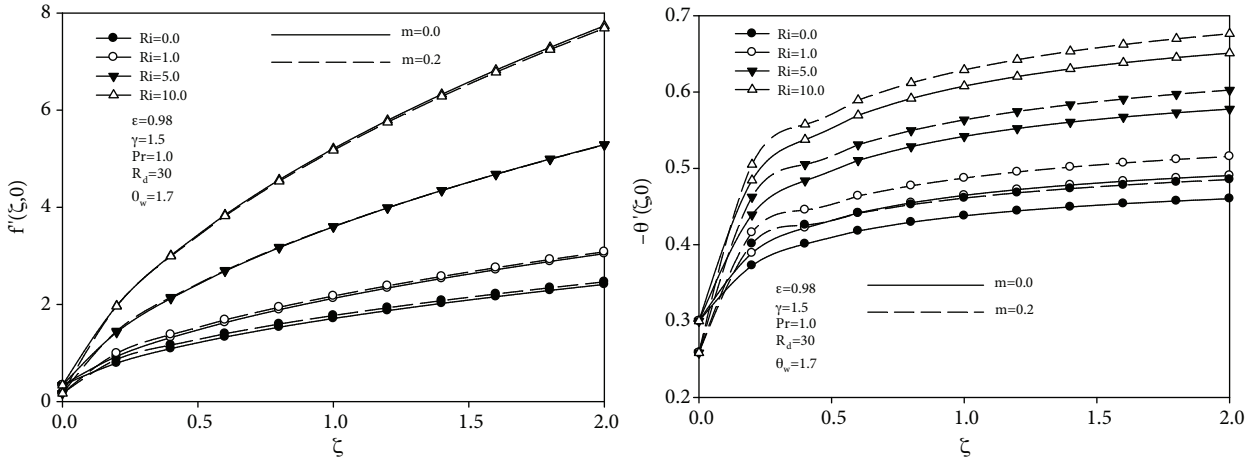

Figure 5. a) Numerical values of local skin friction against the streamwise distance ξ for different values of Ri and m while Pr = 1.0, $\varepsilon = 0.98$, $\gamma = 1.5$, $\mathrm{R}_d = 30$, and $\theta_w = 1.7$. b) Numerical values of local heat transfer parameter against the streamwise distance ξ for different values of Ri and m while Pr =1.0, $\varepsilon = 0.98$, $\gamma = 1.5$, $\mathrm{R}_d = 30$, and $\theta_w = 1.7$.

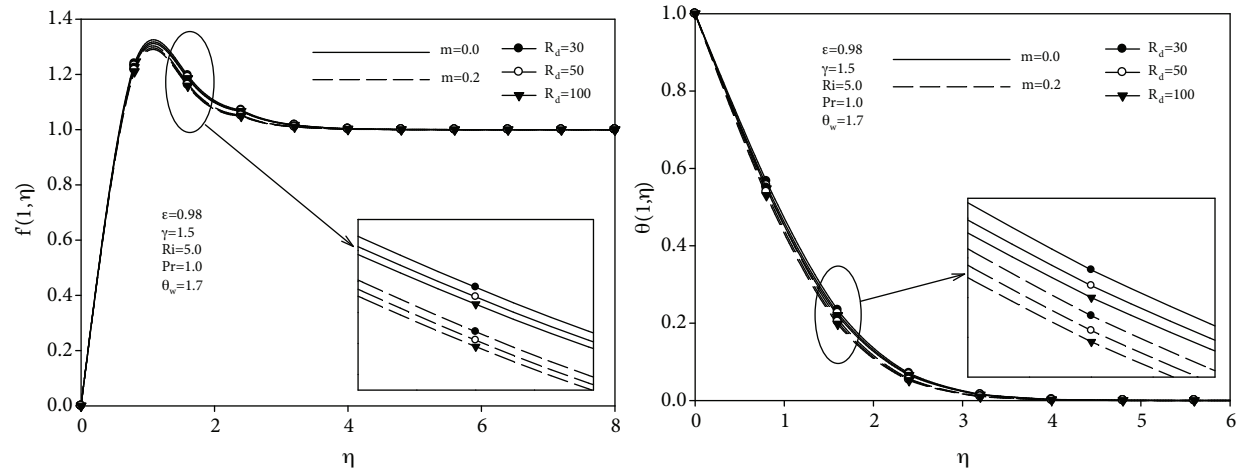

Figure 6. a) Dimensionless velocity profile for different values of R_d and m while Pr = 1.0, $\varepsilon = 0.98$, Ri = 5, $\gamma = 1.5$, $\theta_w = 1.7$, and $\xi = 1.0$. b) Dimensionless temperature profile for different values of R_d and m while Pr = 1.0, $\varepsilon = 0.98$, Ri = 5, $\gamma = 1.5$, $\theta_w = 1.7$, and $\xi = 1.0$.

In Figure 7, the effects of radiation parameter R_d on the local skin friction (Figure 7a) and the local heat transfer (Figure 7b) parameters are displayed for different free stream velocity exponent values of m. Increasing R_d decreases the local skin friction parameter (Figure 7a) and increases the local heat transfer parameter (Figure 7b) as a result of increased hydrodynamic boundary layer thickness and decreased thermal boundary layer thickness.

The effect of surface temperature ratio parameter θ_w on velocity and temperature profiles is shown in Figure 8. Increasing the surface temperature ratio increases dimensionless velocity profile (Figure 8a). Moreover, increasing the temperature ratio also increases the temperatures inside the boundary layer (Figure 8b).

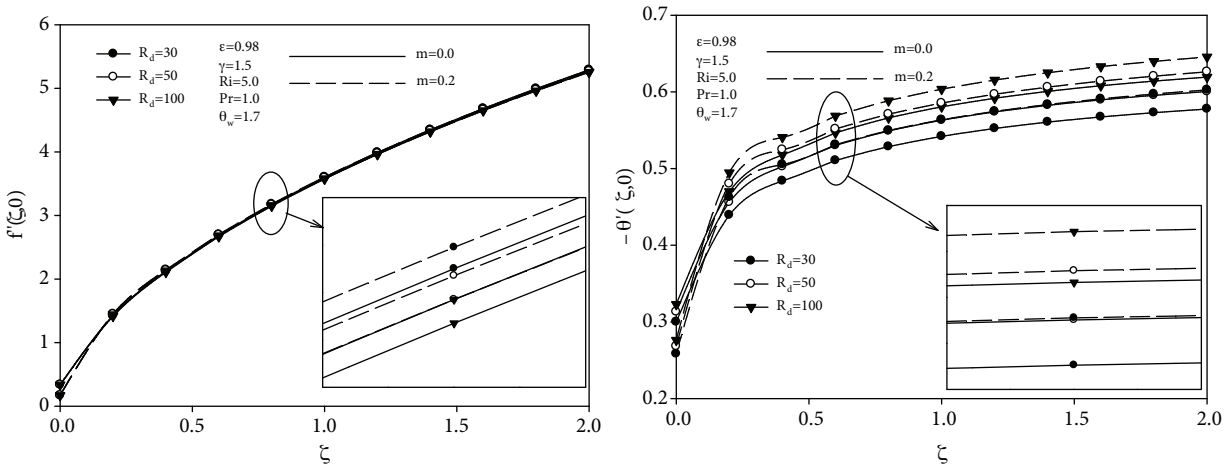

Figure 7. a) Numerical values of local skin friction against the streamwise distance ξ for different values of R_d and m while Pr = 1.0, $\varepsilon = 0.98$, Ri = 5, $\gamma = 1.5$, and $\theta_w = 1.7$. b) Numerical values of local heat transfer parameters against the streamwise distance ξ for different values of R_d and m while Pr = 1.0, $\varepsilon = 0.98$, Ri = 5, $\gamma = 1.5$, and $\theta_w = 1.7$.

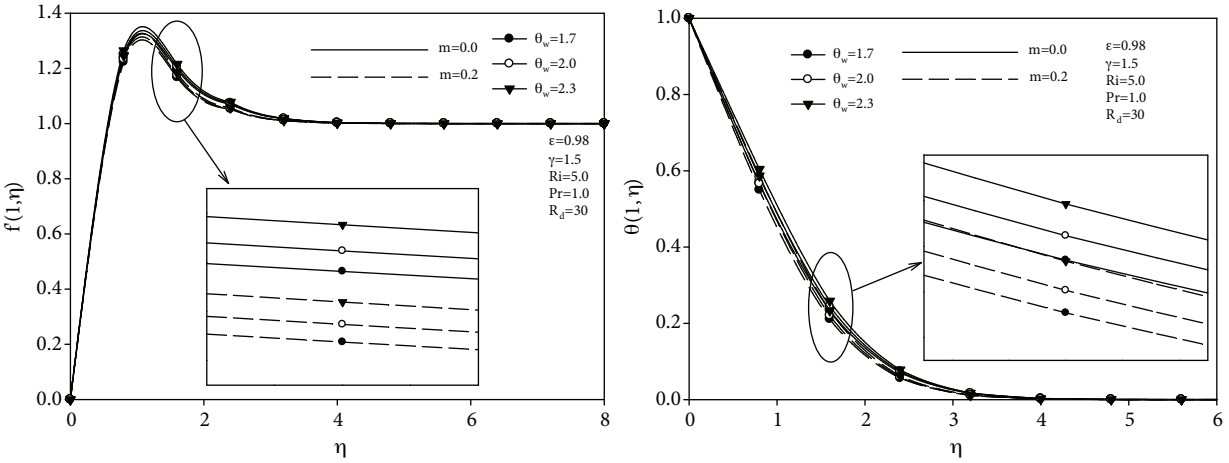

Figure 8. a) Dimensionless velocity profile for different values of θ_w and m while Pr = 1.0, $\varepsilon = 0.98$, Ri = 5, $\mathrm{R}_d = 30$, $\gamma = 1.5$, and $\xi = 1.0$. b) Dimensionless temperature profile for different values of θ_w and m while Pr = 1.0, $\varepsilon = 0.98$, Ri = 5, $\mathrm{R}_d = 30$, $\gamma = 1.5$, and $\xi = 1.0$.

In Figure 9 the effects of surface temperature ratio parameter θ_w on the local skin friction (Figure 9a) and the local heat transfer (Figure 9b) parameters are displayed for different free stream velocity exponent values of m. Increasing θ_w increases the local skin friction parameter (Figure 9a) and decreases the local heat transfer parameter (Figure 9b).

The effect of the Forchheimer parameter γ on the velocity and temperature profiles is shown in Figure 10. Increasing γ and free stream velocity exponent m increases the dimensionless velocity profile (Figure 10a) and decreases the dimensionless temperature profile (Figure 10b).

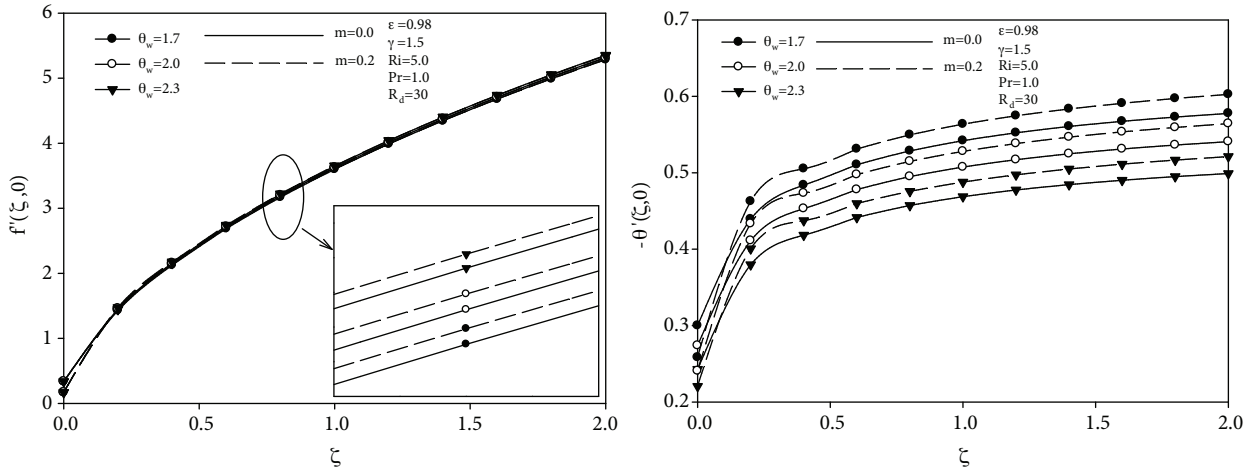

Figure 9. a) Numerical values of local skin friction against the streamwise distance ξ for different values of θ_w and m while Pr = 1.0, ε = 0.98, Ri = 5, R_d = 30, and γ = 1.5. b) Numerical values of local heat transfer parameter against the streamwise distance ξ for different values of θ_w and m while Pr = 1.0, ε = 0.98, Ri = 5, R_d = 30, and γ = 1.5.

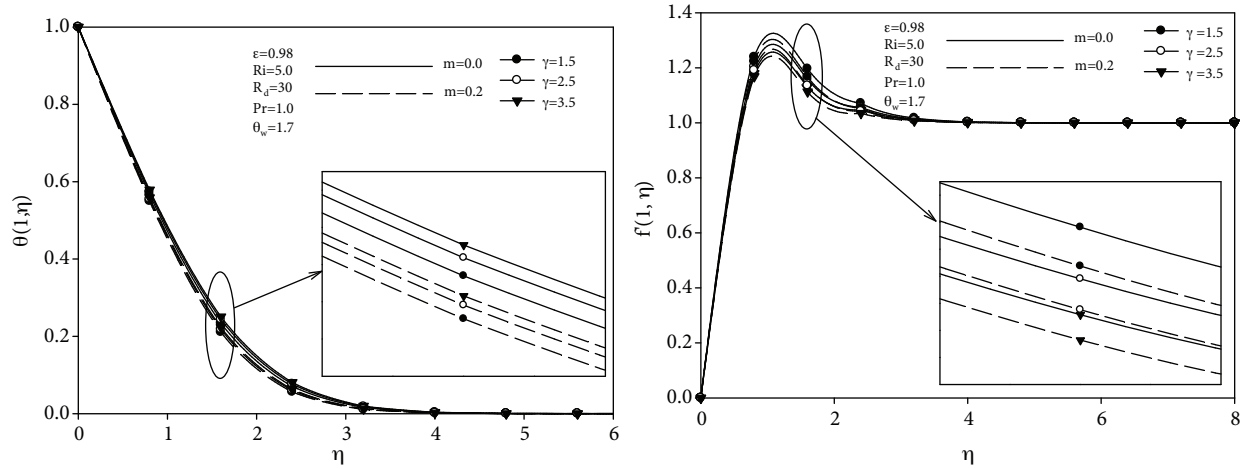

Figure 10. a) Dimensionless velocity profile for different values of γ and m while Pr = 1.0, ε = 0.8, Ri = 5, γ = 1.5, R_d = 30, θ_w = 1.7, and ξ = 1.0. b) Dimensionless temperature profile for different values of γ and m while Pr = 1.0, ε = 0.8, Ri = 5, γ = 1.5, R_d = 30, θ_w = 1.7, and ξ = 1.0.

The effects of Forchheimer parameter γ on the local skin friction and the local heat transfer parameters are shown in Figure 11. The local skin friction (Figure 11a) increases and the local heat transfer (Figure 11b) decreases with an increase in γ.

5. Conclusions

From the present numerical investigation, the following conclusions can be drawn:

1. An increase in the free stream velocity exponent and the radiation parameter decreases the local skin friction parameter and increases the local heat transfer parameter.

2. An increase in the mixed convection increases the local skin friction and the local heat transfer parameters.

3. An increase in the surface temperature parameter and Forchheimer parameter increases the local skin friction parameter and decreases the local heat transfer parameter.

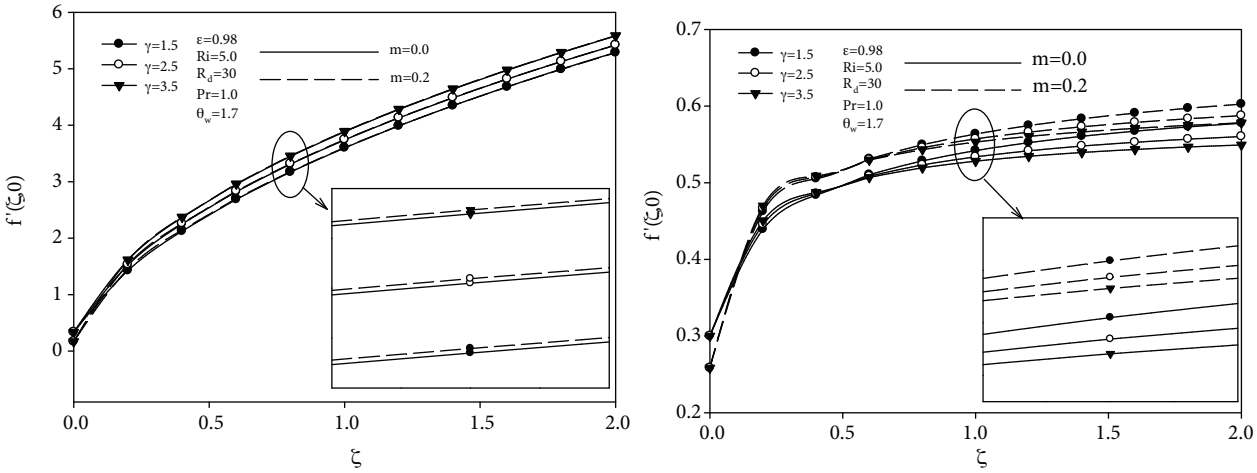

Figure 11. a) Numerical values of local skin friction against the streamwise distance ξ for different values of γ and m while Pr = 1.0, ε = 0.98, Ri = 5, γ = 1.5, R_d = 30, and θ_w = 1.7. b) Numerical values of local heat transfer parameter against the streamwise distance ξ for different values of γ and m while Pr = 1.0, ε = 0.98, Ri = 5, γ = 1.5, R_d = 30, and θ_w = 1.7.

Nomenclature

c_p	Specific heat of the convective fluid
f	Dimensionless stream function
Gr_K	Grashof number based on permeability
k_e	Effective thermal conductivity of porous medium
K	Porous medium permeability
m	Free stream velocity exponent
Pr	Prandtl number
q_R	Component of radiative flux in y direction
r	Radius of the cone
R_d	Radiation parameter
Re_K	Reynolds number based on permeability
T	Temperature
u, v	Velocities in x and y directions, respectively
x, y	Coordinates in horizontal and transverse directions, respectively

Greek symbols

α	Half angle of cone
α_R	Rosseland mean absorption coefficient
β	Coefficient of thermal expansion
ε	Porosity
σ	Stefan–Boltzmann constant
γ	Forchheimer parameter
η	Pseudosimilarity variable, $y\,(U_e/(vx))^{1/2}$
ξ	Nonsimilarity variable, $(vx)/(KU_e)$
ρ	Fluid density
μ	Dynamic viscosity
v	Kinematic viscosity
θ_w	Temperature ratio, T_w/T_∞

Subscripts

w Wall
∞Free stream

References

[1] Kumari M, Nath G. Natural convection from a vertical cone in a porous medium due to the combined effects of heat and mass diffusion with non-uniform wall temperature/concentration or heat/mass flux and suction/injection. Int J Heat Mass Tran 2009; 52: 3064–3069.

[2] Cheng P. Heat transfer in geothermal systems. In: Irvine TF, Harnett JP, editors. Advances in Heat Transfer. New York, NY, USA: Elsevier; 1978. pp. 1–105.

[3] Cheng P. Natural convection in a porous medium: external flow. In: Proceedings of the NATO Advanced Study in Natural Convection. İzmir, Turkey; 1985. pp. 16–27.

[4] Pop I, Ingham DB, Merkin JH. Transient convective heat transfer in external flow. In: Tyvand PA, editor. Advances in Fluid Mechanics. Southampton, UK: Computational Mechanics; 1998. pp. 19–83.

[5] Nield DA, Bejan A. Convection in Porous Media. New York, NY, USA: Springer; 1999.

[6] Vafai K. Handbook of Porous Media. New York, NY, USA: Marcel Dekker; 2000.

[7] Pop I, Ingham DB. Convective Heat Transfer: Mathematical and Computational Modelling of Viscous Fluids and Porous Media. Oxford, UK: Pergamon Press; 2001.

[8] Ingham DB, Pop I. Transport Phenomena in Porous Media. Oxford, UK: Pergamon Press, 2002.

[9] Ravindran R, Roy S, Momoniat E. Effects of injection (suction) on a steady mixed convection boundary layer flow over a vertical cone. Int J Numer Method H 2009; 19: 432–444.

[10] Roy S, Datta P, Mahanti NC. Non-similar solution of an unsteady mixed convection flow over a vertical cone with suction or injection. Int J Heat Mass Tran 2007; 50: 181–187.

[11] Osalusi E, Side J, Harris R, Clark P. The effect of combined viscous dissipation and Joule heating on unsteady mixed convection MHD flow on a rotating cone in a rotating fluid with variable properties in the presence of Hall and ion-slip currents. Int Commun Heat Mass 2008; 35: 413–429.

[12] Ece MC. Free convection flow about a cone under mixed thermal boundary conditions and a magnetic field. Appl Math Model 2005; 29: 1121–1134.

[13] Roy S, Anilkumar D. Unsteady mixed convection from a rotating cone in a rotating fluid due to the combined effects of thermal and mass diffusion. Int J Heat Mass Tran 2004; 47: 1673–1684.

[14] Yih KA. Radiation effect on mixed convection over an isothermal cone in porous media. Heat Mass Transfer 2001; 38: 53–57.

[15] Grosan T, Postelnicu A, Pop I. Free convection boundary layer over a vertical cone in a non-Newtonian fluid saturated porous medium with internal heat generation. Technische Mech 2004; 24: 91–104.

[16] Cheng CY. Soret and Dufour effects on natural convection heat and mass transfer from a vertical cone in a porous medium. Int Commun Heat Mass 2009; 36: 1020–1024.

[17] Chamkha AJ. MHD-free convection from a vertical plate embedded in a thermally stratified porous medium with Hall effects. Appl Math Model 1997; 21: 603–609.

[18] Chamkha AJ, Issa C, Khanafer K. Natural convection from an inclined plate embedded in a variable porosity porous medium due to solar radiation. Int J Therm Sci 2002; 41: 73–81.

[19] Lauriat G, Ghafir R. Forced convective heat transfer in porous media. In: Vafai K, Hadim H, editors. Handbook of Porous Media. New York, NY, USA: Marcel Dekker; 2000. pp. 201–204.

[20] Sparrow EM, Cess RD. Free convection with blowing or suction. J Heat Trans-ASME 1961; 83: 387–396.

[21] Hossain MA, Khanafer K, Vafai K. The effect of radiation on free convection flow of fluid with variable viscosity from a porous vertical plate. Int J Therm Sci 2001; 40: 115–1124.

[22] Yih KA. Mixed convection about a cone in a porous medium: the entire regime. Int Commun Heat Mass 1999; 26: 1041–1050.

[23] Ali MM, Chen TS, Armaly BF. Natural convection–radiation interaction in boundary-layer flow over horizontal surfaces. AIAA J 1984; 22: 1797–1803.

[24] Cebeci T, Bradshaw P. Momentum Transfer in Boundary Layers. Washington DC, USA: Hemisphere; 1977.

[25] Duwairi HM. Viscous and Joule heating effects on forced convection flow from radiate isothermal porous surfaces. Int J Numer Method H 2005; 15: 429–440.

[26] Takhar HS, Beg OA. Effects of transverse magnetic field, Prandtl number and Reynolds number on non-Darcy mixed convective flow of an incompressible viscous fluid past a porous vertical flat plate in a saturated porous medium. Int J Ener Resour 1997; 21: 87–100.

[27] Lloyd JR, Sparrow EM. Combined forced and free convection flow on vertical surfaces. Int J Heat Mass Tran 1970; 13: 434–438.

[28] Chang CL. Numerical simulation of micropolar fluid flow along a flat plate with wall conduction and buoyancy effects. J Phys D Appl Phys 2006; 39: 1132–1140.